Global seismic performance of a new precast CFST column to RC beam braced frame: Shake table test and numerical study

S.Y. Xu [a], Z.L. Li [*], and H.J. Liu [b]

College of civil engineering, Chongqing University, Chongqing 400045, China

Abstract. A new type of precast CFST column to RC beam braced frame is proposed in this paper. A series of shake table tests were conducted to excite a one-third scale six-story model for investigating the global seismic performance of this type of structure against earthquake actions. Particular emphasis was given to its dynamic property, global seismic responses and failure path. Correspondingly, a numerical model built on the basis of fiber-beam-element model, multi-layer shell model and element-deactivation method was developed to simulate the seismic performance of the prototype structure. Numerical results were compared with the measured values from shake table tests to verify the validity and reliability of the numerical model. The results demonstrated that the proposed novel precast CFST column to RC beam braced frame performs excellently under strong earthquake excitations; the "strong CFST column-weak RC beam" and "strong connection-weak member" anti-seismic design principles can be easily achieved; the maximum deflections of precast CFSTC-RCB braced frame satisfied the deflection limitations proposed in national code; the numerical model can properly simulate the dynamic property and responses of the precast CFSTC-RCB braced frame that are highly concerned in engineering practice.

Keywords: precast building; concrete filled steel tubular (CFST) column; reinforced concrete (RC) beam; seismic performance; nonlinear FEM analysis

1. Introduction

In recent years, an increasing number of concrete filled steel tubular (CFST) column to reinforced concrete (RC) beam frames has been constructed. Meanwhile, researches on the connections between CFST columns and RC beams have been also carried out experimentally and theoretically. Nie *et al*. (2008) and Bai *et al*. (2008) studied a new connection system between the CFST column and RC beam, Zhang *et al*. (2012) investigated the seismic behavior of a new type of concrete-filled twin steel tube (CFTST) to RC beam connections. Both of the above two connection systems are through-beam connections, in which the beams directly pass through the panel zone or use other embedded elements to enhance the connection, the weakening of the stiffening and load carrying capacity in the connection zone due to the interruption of the steel tube is compensated by the confinement of the stiffening ring. The above three research results

∗Corresponding author, Professor, E-mail: lizhengl@cqu.edu.cn
[a] Ph.D. Student, E-mail: shuya_xu@cqu.edu.cn
[b] Ph.D., E-mail: lhj20040308@126.com

showed that the connection exhibited good seismic resistance until the beam was totally damaged, and the desired anti-seismic design principles, namely the "strong joint - weak member" and "strong CFTST column - weak beam", could be easily achieved. However, as for the through-beam connection, the CFST column has to be interrupted by the RC beam, and a steel cage made of reinforcement bars has to be anchored to expand the connection region to compensate the reduced stiffness of the composite column. Such connections probably cause difficulties in field construction owing to excessive labor, material and time cost. Sun (2009) conducted a quasi-static test on a single span CFST column to RC beam(CFSTC-RCB) frame, the test results demonstrated that the CFSTC-RCB frame exhibited a good seismic resistance, and the CFST column worked well even until the plastic hinges appeared at the beam ends. Qu (2012) numerically studied the seismic performance of the CFST column to RC beam connections and gave a further understanding of the ultimate state and failure mode of the connections under earthquake actions. Liao *et al*. (2014) conducted a series of cyclic loading tests on the connection between concrete encased column and RC beam, the research results indicated that the connections were dominated by beam failure and had good ductility, that the seismic behavior of the connections is superior to the conventional RC connections but a little bit less favorable than the CFST connections. Li *et al*. (2015) investigated the seismic behavior of the rebar-penetrated connection between gangue concrete filled steel tubular (GCFST) column and reinforced gangue concrete (RGC) beam and found that this type of connection has reasonable strength and rigidity degradation, and follows the "strong column - weak beam" design principle. In addition, this type of structure also has been proven to have good fire resistance (Han *et al*. 2010 and Tan *et al*. 2012).

Excellent seismic performance and fire resistance of CFSTC-RCB connections have been proved by previous investigations. However, research on the global seismic performance of the CFSTC-RCB frame is still very limited.

In addition, existing forms of CFST column to RC beam frames could be only applied in cast-in-place buildings because of their specific construction method. The advantages of precast structures, such as better and controllable quality, faster erection, smaller influence on surroundings compared to cast-in situ structures, make them more appealing in an environmentally friendly, excellent earthquake resistance oriented perspective.

Against above background, this paper proposes a new precast CFSTC-RCB braced frame. To experimentally investigate its seismic performance under earthquake excitations, a series of shake table tests were conducted on a one-third scale six-story test model in the State Key Laboratory of Structural Dynamics of Chongqing Communications Research and Design Institute (CCRDI). Test results, including the dynamic property and responses, are summarized. The failure mechanism was analyzed. Correspondingly, a progressive damage time-history analysis of the prototype structure was carried out based on the fiber-beam-element model, multi-layer shell element model, element-deactivation method to validate the numerical approach to the seismic performance prediction of this type of structure.

2. Description of the proposed new precast CFSTC-RCB braced frame

The precast CFSTC-RCB braced frame adopts square CFST columns, composite beams, and circular CFST braces as its main load carrying system, whose internal steel skeleton is shown in Fig.1. In this braced frame structure, braces cooperate with columns to form dual lateral force resisting system. Braces work as the first resisting system, which is firstly damaged under

earthquake excitations and help the structure dissipate earthquake energy, they can also enhance the lateral stiffness of the structure to decrease the lateral story drift. The strength and stiffness of braces contribution to the whole structure are determined as follows:

Considering a small lateral drift u at the floor and θ is constant (see Fig. 2), the concrete in circular steel tube is used to protecting the brace from buckling in compression, its contribution to force is ignored. The initial lateral stiffness of the brace can be expressed as

$$F_{y,br} = A_{s,br} f_{y,br} \tag{1}$$

Braces yield when the stress of steel tube reach to its yield stress $f_{br,y}$, the lateral force taken by a brace when it yields can be expressed as

$$F_{br,y} = A_{s,br} f_{y,br} \cos\theta \tag{2}$$

The lateral drift of structure when the brace yields can be expressed as

$$u_{br,y} = \frac{F_{br,y}}{k_{br}} = \frac{f_{y,br} \cdot h}{E_{s,br} \sin\theta \cos\theta} \tag{3}$$

It is can be seen from Eq. (3) that the lateral yield displacement of the brace is determined by the yield stress of steel element $f_{br,y}$, θ and story height.
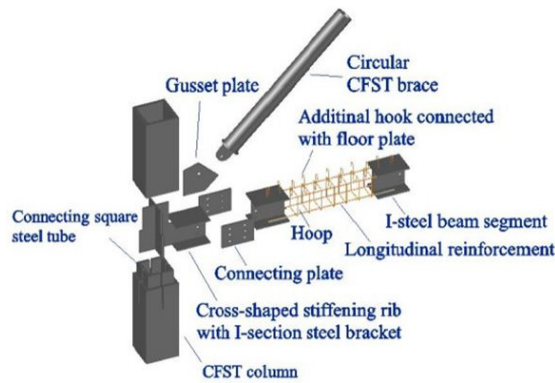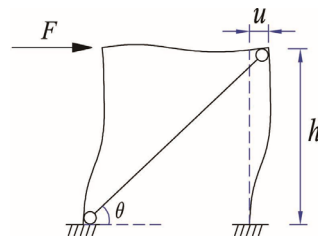

Fig. 1 Internal skeleton of the load carrying system

Fig. 2 Schematic illustration for new braced frame

For example, the common story height of a civil buildings in China is about 3~3.6m, and θ is usually ranges from $30°$~$60°$,the yield stress of Q345 steel is 345 MPa. According to GB 50011-2010, the allowable maximum elasto-plastic inter-story drift angle $\alpha = u/h$ is 1/50. For a structure with a floor height of 3.6 m, 11.83 mm $\leq f_{br,y} \leq$ 13.35 mm. the maximum elasto-plastic inter-story drift of frame is 72 mm according to GB 50011-2010. Apparently, it is easy to achieve the goal that the braces fail before the frame.

The column has a square tube that can confine the concrete. In the column to beam connection region, a connecting square steel tube is used to connect the columns in adjacent floors. The composite beam consists of three beam segments, one RC beam segment and two I-section steel concrete (SC) beam segments, both of the I-section SC beam segments respectively distribute at both ends of the RC beam segment for the purpose of connecting the beam end with the CFST column to form column-beam connection. A stiffening rib with cross-shaped section is embedded into the top end of the column to enhance the connection region, making the connection region stronger than the structural members it connects. The cross-shaped stiffening rib has I-Section steel brackets that can connect with the composite beams using connecting plates. Circular CFST

(a) Setting up the square steel tube and stiffening rib

(b) Positioning the composite beam

(c) Forming column to beam connections

(d) Forming column to beam connections

(e) Installing CFST braces

(f) Seating the precast layer of the floor plate on beam

(g) Arranging reinforcements in cast-in-place layer

(h) Molding and concreting
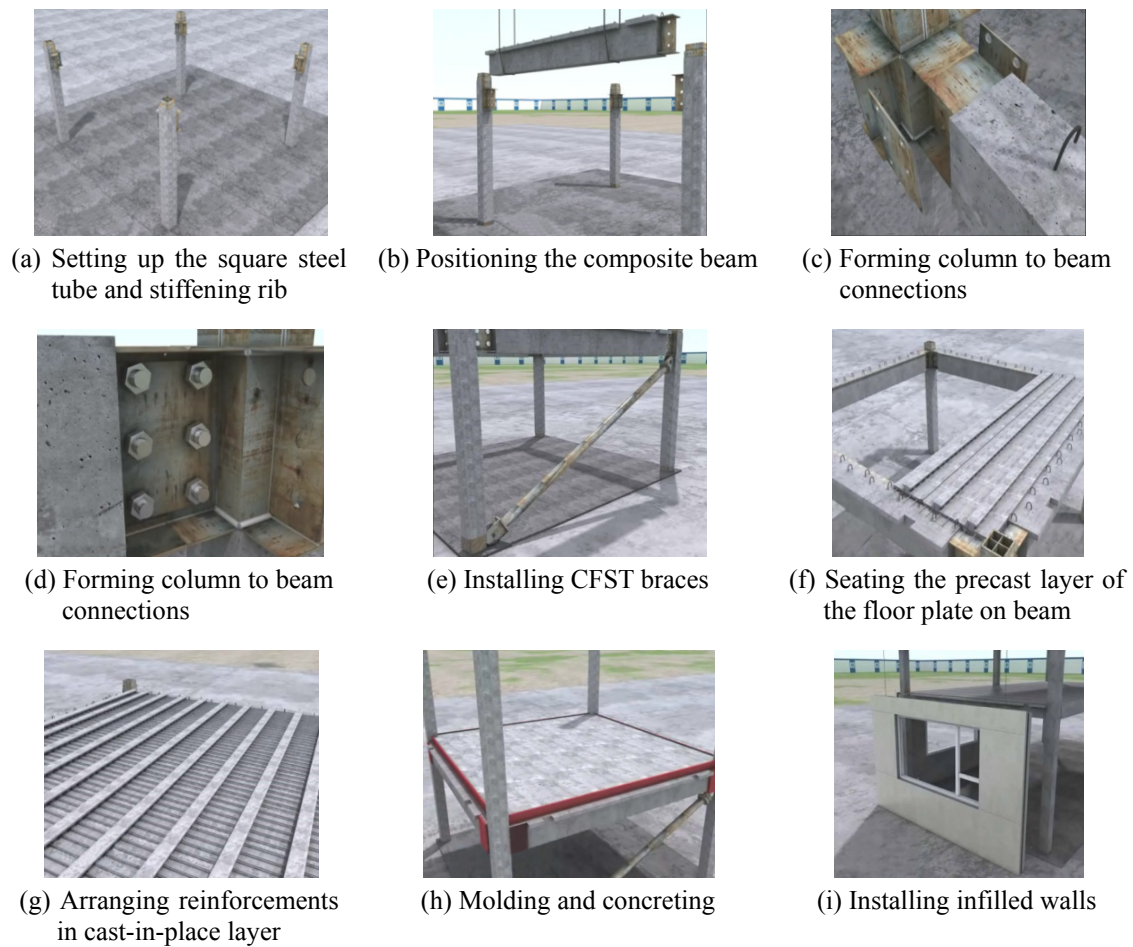
(i) Installing infilled walls

Fig. 3 Construction procedures

braces connect to the column to beam connection by gusset plate. The floor plate is superimposed slab that consists of a precast layer and a cast-in situ layer (see Fig. 6), its longitudinal and transverse reinforcements connect with the additional hooks extended from the composite beam tightly to form the connection between the beam and floor plate.

The vast majority of structural members are produced in precast plants, including the square steel tube, composite beam, CFST brace, cross-shaped stiffening rib, connecting plate and bottom layer of laminated slab, leaving a small quantity of assembly, welding and concreting conducted on site.

Construction of the precast CFSTC-RCB braced frame is executed using the following procedures:

(1) embedding the cross-shaped stiffening rib into the top end of the square steel tube and welding the seams using full-length welding;
(2) connecting the square steel tube in upper floor to the one in lower floor or base (see Fig. 3(a));
(3) connecting the composite beam to the CFST column, the web plates are connected using high-strength bolts and the flanges are connected using full-fillet welds(see Fig. 3(b), (c), (d));
(4) installing circular CFST braces (see Fig. 3(e));
(5) positioning the precast layer of the floor plate onto the beam (see Fig. 3(f));
(6) arranging the transverse reinforcements of the cast-in-place layer of the floor plate (see Fig. 3(g));
(7) using cast-in-place concrete to fill the square steel tube and the cast-in-place layer of the floor plate, grouting the splicing closure (see Fig. 3(h));
(8) installing in-filled walls according to the construction drawing after every 3 to 5 stories' erection (see Fig. 3(i)).

3. Test structure

3.1 Prototype structure

The prototype structure designed for case study was a 6-story precast CFSTC-RCB braced frame depicted in Fig. 4. It had a regular rectangular shape consisting of four frames with the span of 5.2 m in the longitudinal direction(X-direction) and three frames with the bay of 2.4 m in the transverse direction(Y-direction). The columns cross-section was constant along the height. The CFST braces had the same cross-section, while the gusset plates had different geometries due to the different length of the spans. RC beams in X- and Y- directions were marked with "L-1" and "L-2", respectively. Beams with the same marks had the same cross-section. Typical connection details are shown in Figs. 5-7. The overall design of the prototype was executed according to the Chinese national codes (see GB 50010-2010, GB 50011-2010 and GB 50017-2003). On the basis of 63%, 10% and 2% probabilities of earthquake occurrences over a 50-year design recurrent period, the peak ground accelerations (PGAs) of frequent, occasional and rare earthquake levels were 0.035 g, 0.10 g and 0.22 g respectively (g represents the gravity acceleration). θ in X- and Y- directions are respectively $34.69°$ and $45°$, $u_{br,y}$ in X- and Y- directions are respectively 12.64 mm and 11.83 mm According to Eq. (3).

The concrete used in the prototype structure was grade C30 concrete (cubic compression

(a) Plan view   (b) Elevation views
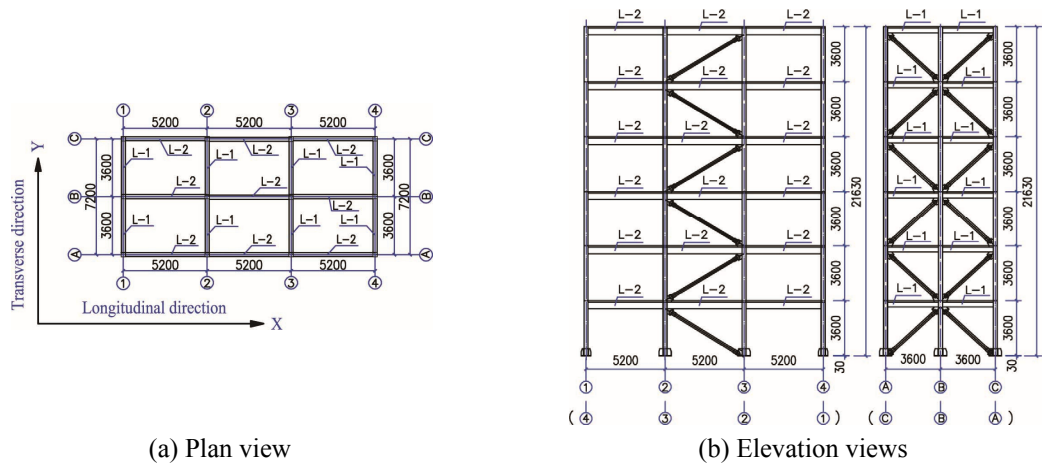
Fig. 4 Structural layout of prototype

* Dimension in mm
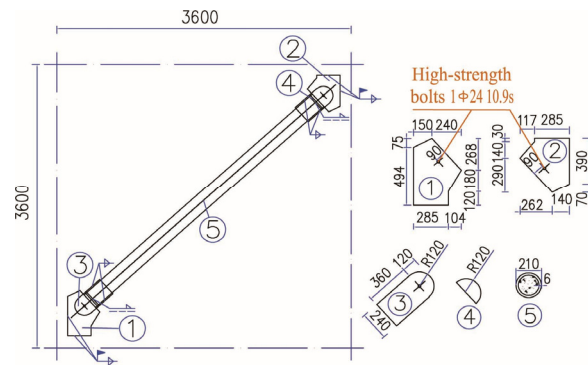
Fig. 5 Details of typical brace connection

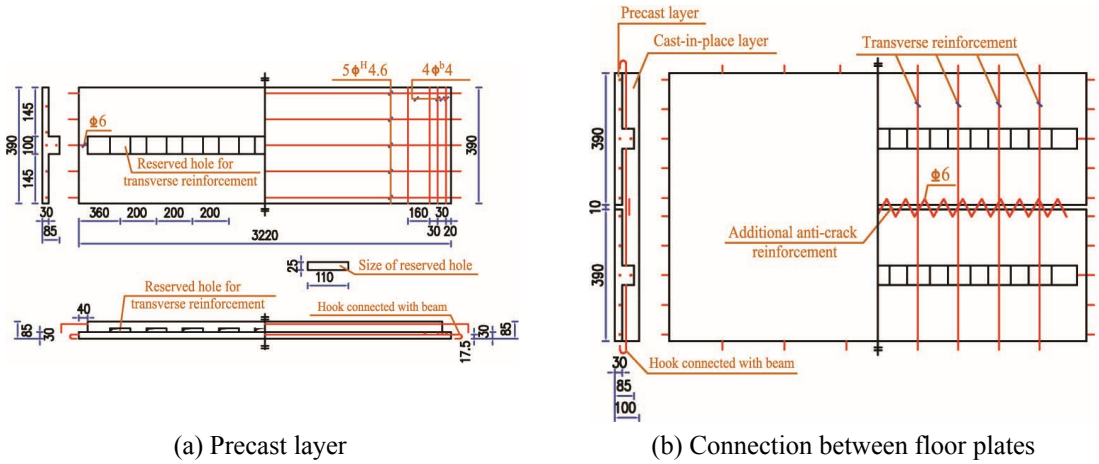* Dimension in mm. The thickness of steel elements is 9 mm

(a) Precast layer   (b) Connection between floor plates

Fig. 6 Details of superimposed floor plates (dimension in mm)

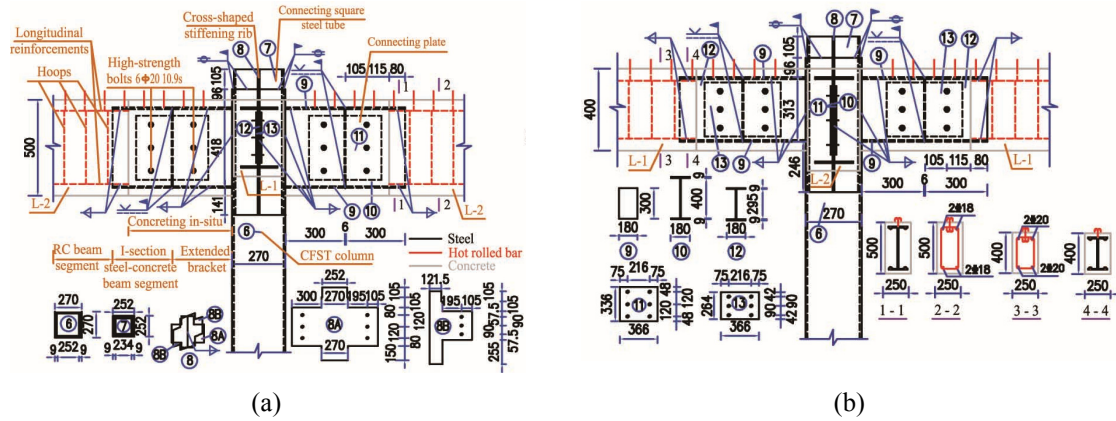(a)   (b)

Fig. 7 Details of typical CFST column to RC beam connection
* Dimension in mm. The thickness of steel elements is 9 mm

strength f_{ck} = 30 N/mm^2) whereas the longitudinal and transverse reinforcements, hoops, and steel elements were designed with grade HRB400 (yield stress f_y = 400 N/mm^2), grade HPB300 hot rolled bars (f_y = 300 N/mm^2) and grade Q345 steel (f_y = 345 N/mm^2), respectively.

3.2 Test model

The similitude law was considered in the design of the scaled test model as listed in Table 1. For purposes of reducing the error brought by scale effects and clearly observing the damage occurred during seismic excitations, it would be good to choose a large-scale model other than a small one. Considering the capacities of the shake table facility and crane, a one-third scale model was finally selected.

Table 1 Similitude scale factors for test model

Parameter	Similitude Scale Factors
Length	S_l=1/3
Elastic modulus	S_E = 0.823
Acceleration	S_a = 2.000
Shear strain	$S_\varepsilon = S_\sigma/S_E$ =1
Time	$S_T = S_l^{0.5} \bullet S_a^{-0.5}$ = 0.408
Frequency	S_f=1/ S_T = 2.451
Equivalent density	$S_\rho = S_\sigma/(S_a \bullet S_l)$ =1.235
Mass	$S_m = S_\sigma \bullet S_l^2/S_a$=0.046
Displacement	S_d = S_l=1/3
Stress	S_σ = S_E = 0.823
Axial force	$S_F = S_\sigma \bullet S_l^2$=0.091

* The similarity ratio S = the test model value / the prototype structure values

Table 2 Measured material properties

Steel and reinforcement	E_s (MPa)	f_{sy} (MPa)	f_{su} (MPa)	Concrete	E_c (MPa)	f_{cu} (MPa)
Column tube	2.02×10^5	311	488	Base	2.93×10^4	25.77
Brace tube	2.00×10^5	326	465	Column	2.45×10^4	25.90
I-steel girder	2.00×10^5	355	441	Brace	2.32×10^4	21.03
Gusset plate	2.00×10^5	355	507	Beam	2.32×10^4	21.03
Longitudinal reinforcement	2.06×10^5	405	545	Plate	1.71×10^4	17.87
Hoops	1.99×10^5	289	402			

The test model was cast using fine gravel concrete. The reinforcements with a less than 5 mm diameter, including the hoops and additional hooks in beams and the reinforcements in floor plates, were replaced by galvanized steel wires. Except for the fine gravel concrete and galvanized steel wire, the rest of the materials used in test model are as same as the ones used in prototype structure. Table 2 summarizes the measured properties of the materials used in test model.

Considering the live load on floor (2.0 kN/m²) suggested by the load code for the design of building structures (GB 50009-2012) and decoration load (0.5 kN/m²), the equivalent total mass of prototype structure is 465.912 t. According to mass similitude scale factor, additional lead weights weighed 6.77 t were added to each floor to satisfy the mass similitude requirement, bring the total weight of the model, including the base with a weight of 4.78 t, to 26.05 t. The base of the test model was attached firmly to the shake table surface with 21 grade 10.9 s high-strength bolts with a diameter of 28 mm.

The completed model is shown in Fig.8 as it sat on the shake table in the State Key Laboratory of Structural Dynamics of CCRDI.

4. Test setup and procedures

The shaking table tests were conducted in the State Key Laboratory of CCRDI. The main experimental device was a shaking table array with two shake tables, shown in Fig. 9. The closer one is a fixed table, while the farther one is movable. Detailed capacity of the shake table array is listed in Table 3. The shake table tests were conducted on the fixed table.

For the purpose of studying the seismic performance of the test model in a wide range from elastic to elasto-plastic, test was carried out in 5 consecutive stages with increasing PGA, and loading cases of longitudinal input and transverse input were considered in each stage as list in Table 4. The first three stages were corresponding to frequent, occasional and rare earthquake levels, while Stage 4 and 5 were considered as extremely rare earthquake levels that were not demanded in the GB 50011-2010. Stage 4 and 5 were optional stages carried out to pose more severe damage to the test model up until the test model could not sustain a higher level of earthquake intensity. Nature frequencies and mode shapes of the test model were identified by using stochastic subspace identification (SSI) method (Li 2009) from the acceleration responses to a white noise excitation at the beginning of the shake table tests and at the end of each direction of every stage.

Shake table tests were carried out respecting the testing protocol proposed by GB 50011-2010:
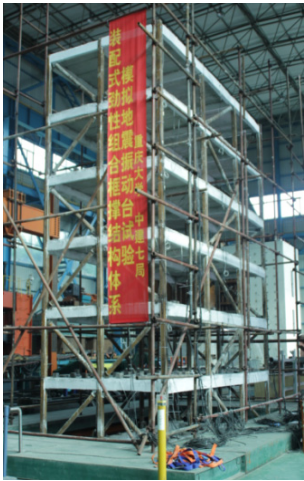
Fig. 8 Test model

Fig. 9 Shake table array in CCRDI

Table 3 Capacity of the shake table array in CCRDI

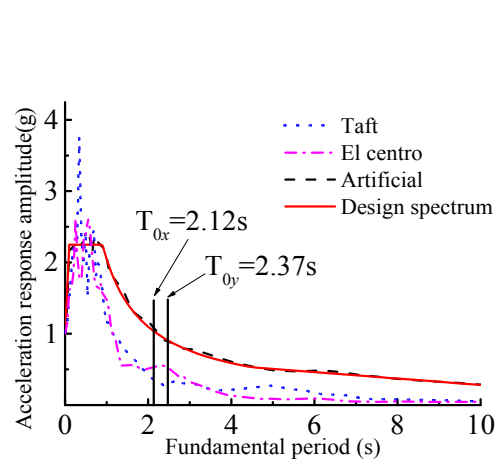| Parameter	Capacity
Payload (ton)	2×35
Size (m)	2×3×6
Degree of freedom	6
Max Disp (mm)	X/Y(horizental): ±150 mm / Z(vetical): ±100 mm
Max Vel (m/s)	X/Y:0.8 Z:0.6
Max Accel (g)	X/Y/Z: ±1.0dc
Max Freq (Hz)	0~±50

Fig. 10 Acceleration spectra of selected excitations
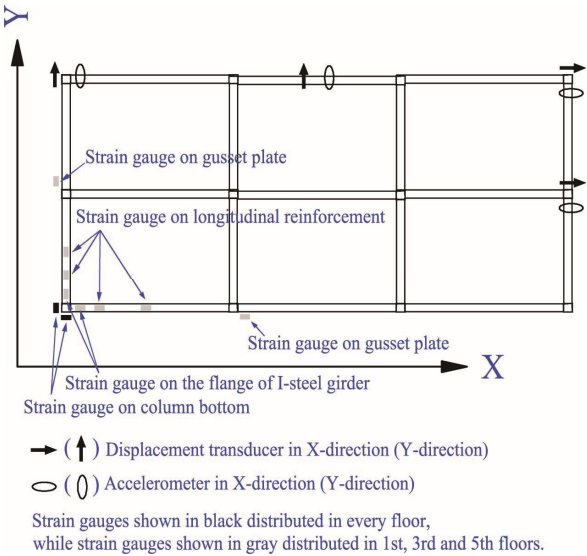

Fig. 11 Arrangement of measuring transducers

Table 4 Test procedure

Stage	Direction	Excitation	Desired PGA(g)	Measured PGA(g)
Initial	-	White noise	0.05	-
1	X	Taft	0.07	0.079
	X	El Centro	0.07	0.075
	X	Artificial	0.07	0.071
	-	White noise	0.05	-
	Y	Taft	0.07	0.076
	Y	El Centro	0.07	0.080
	Y	Artificial	0.07	0.073
	-	White noise	0.05	-
2	X	Taft	0.2	0.220
	X	El Centro	0.2	0.196
	X	Artificial	0.2	0.202
	-	White noise	0.05	-
	Y	Taft	0.2	0.223
	Y	El Centro	0.2	0.192
	Y	Artificial	0.2	0.212
	-	White noise	0.05	-
3	X	Taft	0.44	0.438
	X	El Centro	0.44	0.451
	X	Artificial	0.44	0.418
	-	White noise	0.05	-
	Y	Taft	0.44	0.470
	Y	El Centro	0.44	0.442
	Y	Artificial	0.44	0.451
	-	White noise	0.05	-
4	X	Taft	0.62	0.630
	X	El Centro	0.62	0.652
	X	Artificial	0.62	0.656
	-	White noise	0.05	-
	Y	Taft	0.62	0.691
	Y	El Centro	0.62	0.581
	Y	Artificial	0.62	0.667
	-	White noise	0.05	-
5	X	Taft	0.8	0.836
	-	White noise	0.05	-

two naturally recorded seismic waves (Taft wave and El Centro wave) and one artificial seismic wave generated according to the design response spectrum were used as seismic excitations. Initial fundamental frequencies in X- and Y- directions were obtained before the tests. According to the

acceleration spectra of these three selected waves, the input sequence of earthquake excitations at each stage was Taft wave, El Centro wave and artificial wave (see Fig. 10, where T_{0x} and T_{0y} were the initial fundamental period in X- and Y- directions, respectively), it was determined in such a way that the acceleration responses of test model were amplified gradually as the test progressed.

The test model and the table surface were instrumented with 28 accelerometers, 26 displacement transducers and 36 strain gauges to capture the dynamic responses as shown in Fig. 11.

The table surface and the base of test model were respectively instrumented with two accelerometers to measure the acceleration responses in the X- and Y- directions. Four accelerometers were mounted on every floor level to measure the acceleration responses in X- and Y- directions and obtain the torsion responses. Two displacement transducers were installed on the base of test model and four displacement transducers were placed on every floor level to measure the displacement responses and obtain the torsion responses.

5. Test results

5.1 Observation

As the PGA of seismic excitation increased from 0.07 g to 0.20 g, the test model responded with a visible tremor and vibrated like a rigid body, the maximum relative displacement between the roof and the base is 6.64 mm. All the structural members worked well and no visible damage was observed.

When test model subjected to the excitations with a PGA of 0.44 g in X-direction, some micro-cracks were found at the interface between the RC beam segment and SC beam segment of the beams in X-direction. During the artificial excitation, the gusset plate connected to the longitudinal circular CFST brace on axis A in the 2nd floor deformed, then the high-strength bolt cut, which resulted in that the circular CFST brace quitted working. The maximum relative displacement at the roof was 16.77 mm.

When subjected to the excitations with a PGA of 0.44 g with a PGA of 0.44 g in Y-direction, other two braces quitted working (see Fig. 23). Cracks began to appear on the interface between the RC beam segment and SC beam segment of the beams in Y-direction. The maximum relative displacement at the roof was 33.36 mm.

When subjected to earthquake excitations with a PGA of 0.62 g, test model vibrate much more violently. It was clearly observed that the vibration amplitude of test model to different types of excitations with a same PGA were different, the vibration response to the artificial excitation was most violent, the vibration response to the El Centro excitation was second, and the one to the Taft excitation was most slight. The protective layer concrete of the SC beam segment spall off from the beam body due to the absence of shear tubs. The cracks at the interface between the RC beam segment and SC beam segment developed obliquely down to beam bottom, forming through cracks. It is important to note here that the composite beams, which were adjacent to the failed braces, were visibly under more severe damage compared with the ones that were not. The propagation of cracks at the interface between the RC beam segment and SC beam segment was followed by the yielding of the composite beam, while the CFST columns and the column to beam connections maintained a very stable status. Cracks were also observed at the bottom of some floor plates from this stage onwards.

816   *S.Y. Xu, Z.L. Li and H.J. Liu*

When subjected to Taft excitations with a PGA of 0.80 g in X-direction, large quantities of concrete blocks and some braces fell off from the test model, beams and braces were more severely damaged, while the CFST columns and the column to beam connections still sustained excellent performance.

During the shake table tests, no brace in 1st floor failed, it should be due to that the column bases made a great contribution to the lateral stiffness, which reduced the inter-story drift in the 1st floor.

5.2 Failure path

Damage started with the appearance of some micro-cracks at the interface between the RC beam segment and SC beam segment of composite beams. As the earthquake excitations intensified, some CFST braces in the floor, where inter-story drift was relatively high, failed. Then plastic hinges appeared on the composite beams that were adjacent to the failed braces and through cracks were found on the bottom of some floor plates. In the whole process of shake table tests, the CFST columns and the column to beam connections worked well. The failure order of the load carrying system was brace first, RC beam second and CFST column third. The failure path of the precast CFSTC-RCB braced frame indicated that this type of structure could follow the "strong joint - weak member" and "strong CFST column - weak RC beam" anti-seismic design principles.

5.3 Dynamic property

The 1st order fundamental frequencies and first two order mode shapes for different stages are shown in Figs. 12-13, respectively. Fig. 12 indicates that the fundamental frequencies decreased with the increasing of the PGA. The fundamental frequencies showed no obvious change in first two stages, which indicated that the test model stayed in elastic condition. Since Stage 3 where braces started to quit working, the fundamental frequency decreased obviously, which showed that braces contribute a lot to the lateral stiffness of whole structure. Moreover, when test model subjected to the excitations in X-direction, the fundamental frequency in X-direction decreased more dramatically than that in Y-direction, which revealed that the excitations in X-direction had a greater effect on the structural members along the X-direction, and vise versa. The initial
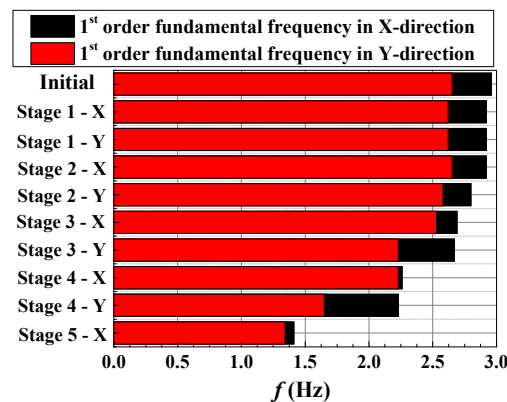

Fig. 12 Change in fundamental frequency of test model

(a) 1st order mode shape in X-direction

(b) 2nd order mode shape in X-direction

(c) 1st order mode shape in Y-direction

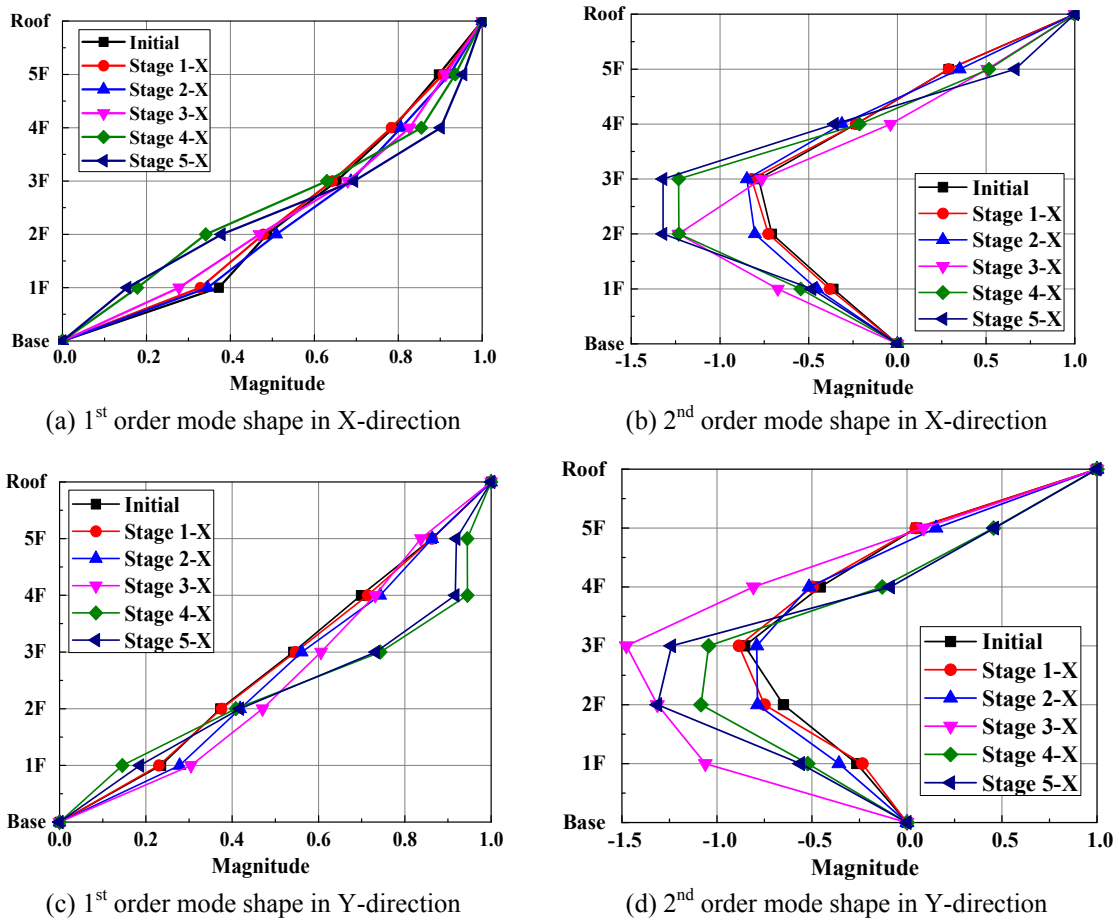(d) 2nd order mode shape in Y-direction

Fig. 13 Change in mode shape

fundamental frequencies in X- and Y- directions were 2.96 Hz and 2.65 Hz, respectively. After the shake table tests, the fundamental frequencies in X- and Y- directions respectively decreased to 1.41 Hz and 1.34 Hz.

At the beginning of the test, the mass and stiffness uniformly distributed at each floor, 1st order mode shapes in X- and Y- directions were approximate to straight lines. It can be known from the observation that the second and third floors were more early and severely damaged than other floors, more remarkable stiffness degradation happened to these two floors, so that the 1st order mode shape began to bend obviously since Stage 4. In addition, the 2nd order mode shape in the second and third floor deviated dramatically from its initial value under rare and extremely rare earthquakes.

5.4 Acceleration response

The amplification factor of acceleration is an important index reflecting the structural dynamic response. The amplification factor of acceleration at floor *i* is defined as
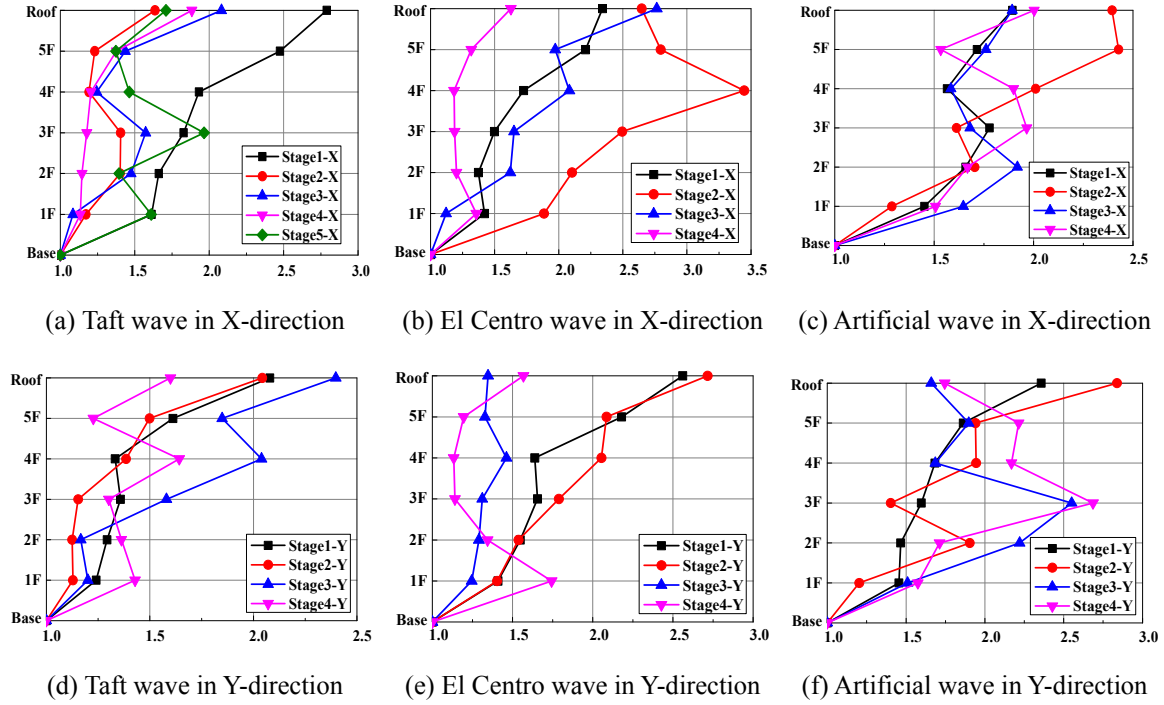
S.Y. Xu, Z.L. Li and H.J. Liu

(a) Taft wave in X-direction (b) El Centro wave in X-direction (c) Artificial wave in X-direction

(d) Taft wave in Y-direction (e) El Centro wave in Y-direction (f) Artificial wave in Y-direction

Fig. 14 Amplification factors of acceleration of test model

(a) Taft wave in X-direction (b) El Centro wave in X-direction (c) Artificial wave in X-direction

(d) Taft wave in Y-direction (e) El Centro wave in Y-direction (f) Artificial wave in Y-direction
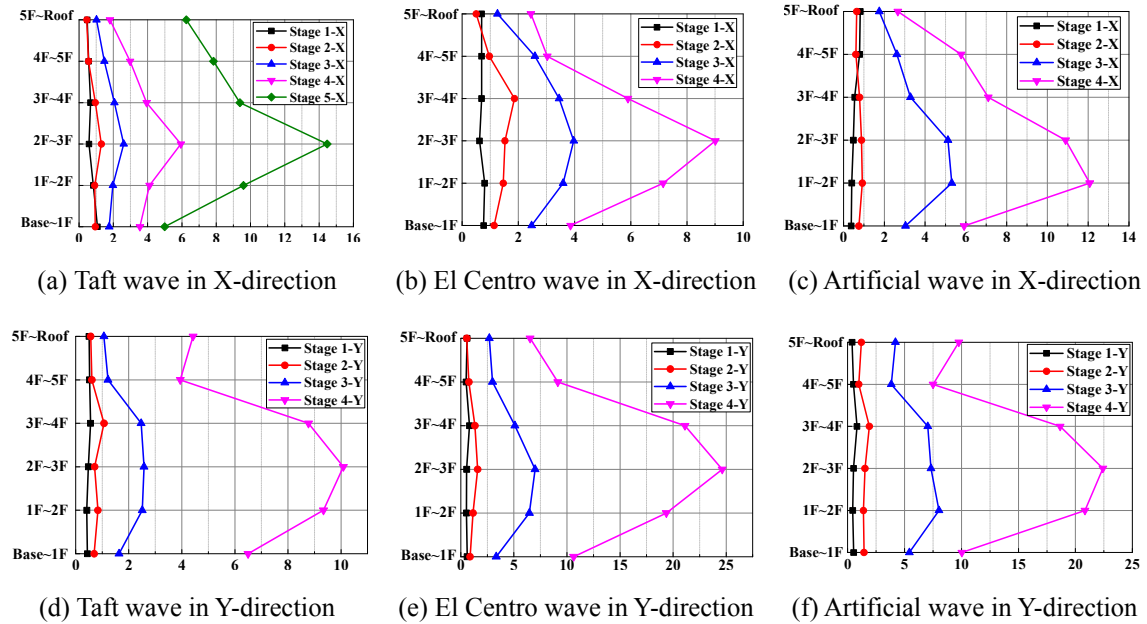
Fig. 15 Maximum inter-story deflection of test model

$$\alpha_i = \frac{\max(\ddot{x}_i(t))}{\max(\ddot{x}_g(t))} \tag{4}$$

Where $\ddot{x}_g(t)$ is the time history of the acceleration of ground motion; $\ddot{x}_i(t)$ is the time history of the acceleration in the floor i.

Fig. 14 illustrates the amplification factors of acceleration under different levels of earthquake excitations. The amplification factors of acceleration from earthquake excitations with different PGA had no obviously growth or downward trend as the PGA increased. Generally, in the stage where PGA of the earthquake excitation was relatively low, such as Stage 1 and 2, the amplification factor increased with the height. However, in the stage where PGA of the earthquake excitation was relatively high, such as Stage 4, the amplification factor increased in the floors where the lateral stiffness dramatically decreased.

5.5 Displacement and torsion responses

Fig. 15 shows the maximum inter-story deflection of test model under different seismic intensities. As it can be seen from the Fig. 15 that, the maximum inter-story deflection increased with the increasing of PGA. At Stage 1 and 2, very little inter-story deflection was measured. From Stage 3 where CFST brace system started failing, the inter-story deflection of 2nd, 3rd and 4th floors are obviously larger than that of the 1st, 5th and 6th floors. The maximum inter-story drift angles of test model at each stage are listed in Table 5. According to GB 50011-2010, the allowable maximum inter-story drift angle under frequent and rare earthquake, namely the allowable maximum elastic inter-story drift angle and maximum elasto-plastic inter-story drift angle, are 1/550 and 1/50, respectively. In the shake table test, maximum elastic inter-story drift angle and maximum elasto-plastic inter-story drift angle were respectively 1/1119 and 1/149, which satisfied the proposed deflection limitations of the Chinese national code. Results also showed that when test model subjected to extremely rare earthquake excitations that were not required by national code but conducted in this tests, the maximum inter-story drift angle was 1/49, which surpassed the allowable maximum inter-story drift angle, the composite beams and the CFST braces were under severe damage but the CFST columns and column to beam connections still exhibited good
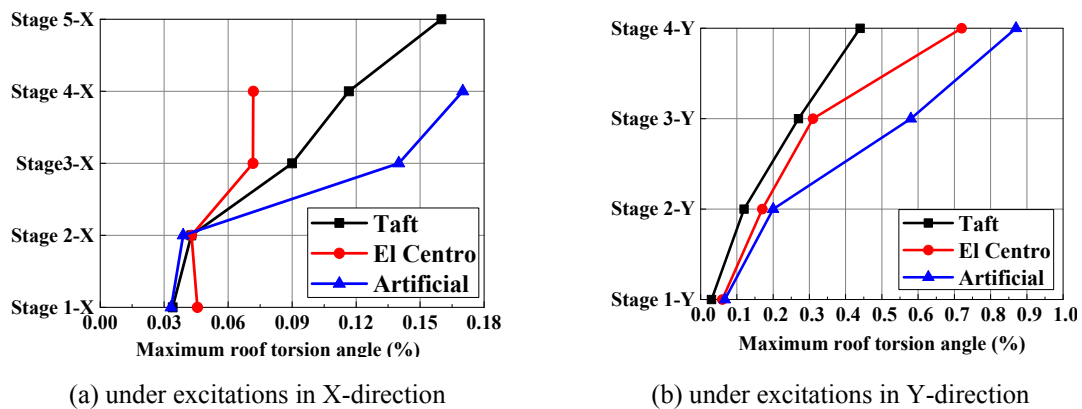

(a) under excitations in X-direction   (b) under excitations in Y-direction

Fig. 16 Maximum inter-story deflection of test model

Table 5 Maximum inter-story drift angle of test model

Stage	Direction	Maximum inter-story drift angle	Location	Excitation
1	X	1/1119 in X direction	5F~6F	Taft wave
	Y	1/1460 in Y direction	3F~4F	Artificial wave
2	X	1/625 in X direction	3F~4F	El Centro wave
	Y	1/625 in Y direction	3F~4F	El Centro wave
3	X	1/227 in X direction	1F~2F	Artificial wave
	Y	1/149 in Y direction	1F~2F	Artificial wave
4	X	1/99 in X direction	1F~2F	Artificial wave
	Y	1/49 in Y direction	2F~3F	El Centro wave
5	X	1/83 in X direction	2F~3F	Taft wave

* Excitation represents the excitation under which the maximum inter-story drift angle appeared

load carrying capacity. From stage 3, the maximum inter-story drift exceeds the yield inter-story drift of braces, which indicates that the braces yield before the cut of the bolt connections of braces, the cut of bolts should be due to fatigue failure under seismic loads, the form of bolted connections should be further optimized to maximize the energy dissipating capacity of braces. Fig. 16 shows the maximum roof torsion angle under different levels of excitations in X- and Y- directions, the maximum roof torsion angle under the same type of excitation in the same direction increased as the PGA increased. In general, the maximum roof torsion angle responses from the excitations in Y-direction were much greater than these from the excitations in X-direction.

6. Dynamic responses of the prototype

In order to validate the numerical method of the seismic performance prediction of PCFSTC-RCB braced frame, a numerical model of the prototype structure is built on the basis of fiber-beam-element model, multi-layer shell element model and element-deactivation method. A time history analysis on the numerical model is conducted, whose results are compared with the test values obtained from the shake table tests.

6.1 Numerical model

6.1.1 Fiber-beam-element model and multi-layer shell model
The fiber-beam-element and multi-layer shell element model have been proved as very effective computing elements and have been widely used in global dynamic response analysis. In particular, these two models have been successfully used in the progressive collapse analysis of building structures in recent years. Lu *et al.* (2008, 2009 and 2012) successfully developed the fiber-beam-element and multi-layer shell element numerical model that are compatible with the commercial software MSC.MARC and numerically investigated the earthquake-induced collapse behaviors of building structure. In the fiber-beam-element model, a beam section is divided into a number of fibers, whose material properties are described with uniaxial stress-strain model. In a beam section, the deformation between fibers follows plane section assumption. In this numerical analysis, the numerical elements of composite beams, CFST columns and CFST braces were

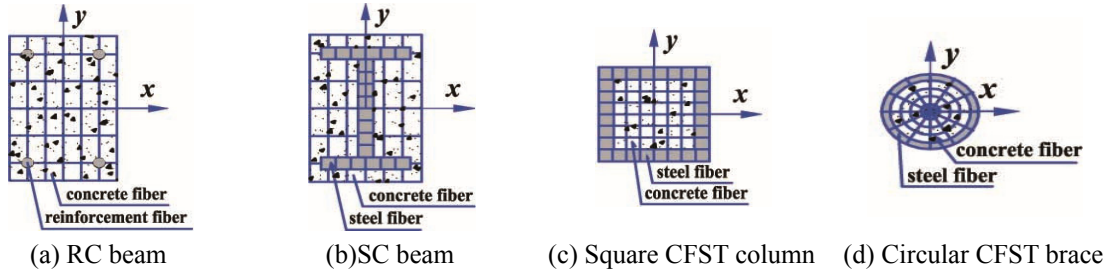(a) RC beam   (b)SC beam   (c) Square CFST column   (d) Circular CFST brace

Fig. 17 Fiber distribution in a section

developed based on the fiber-beam-element model, fiber distribution in these sections are illustrated in Fig. 17. The numerical elements of floor plates were modeled with multi-layer shell elements, each floor plate was divided into a number of layers in the thickness direction. The reinforcing bars in floor plates were defined as the equivalent steel layers based on the actual reinforcement ratio. Each floor plate was divided into 4 steel layers and 6 concrete layers. Element 52 (straight Euler-Bernoulli beam) and element 140 four-node hick-shell element) in the element library of MSC.MARC (2010a) were respectively selected to model the beam elements and shell elements.

In addition, according to the shake table tests, the circular CFST brace system was under progressive failure, which resulted in noteworthy lateral stiffness degeneration of the whole structure and should be carefully considered in the numerical analysis. Therefore, the UACTIVE user subroutine was developed based on element-deactivation method and inserted into the MSC.MARC (2010b) to deactivate the brace element when its axial force surpassed 1.05 times of its yield axial force. A deactivated brace element does not contribute to the load, mass, stiffness, or internal force calculation any longer and its stress and strain are reset to zero.

6.1.2 Material properties

The mechanical properties of concrete confined by reinforcements and steel elements can be very different. In current study, Wang XL concrete constitutive model (as proposed by Wang *et al*. 2007), which was modified base on Légeron concrete constitutive model (see Légeron and Paultre 2003), and Han LH model (as proposed by Han *et al*. 2001) were respectively selected as the concrete constitutive models for the concrete in RC elements and CFST elements. In addition, loading and unloading constitutive model of concrete proposed by Légeron and Paultre (2003) was used in numerical simulation taking account of the cracking, stiffness degrading and hysteretic loading behavior of concrete. As for steel material, Wang XL steel constitutive model (as proposed by Wang *et al*. 2007), which was developed on the basis of Légeron steel constitutive model (see Légeron and Paultre 2003) was adopted. These material constitutive models have been proven as very proper and effective material models for corresponding structural elements in numerical analysis as reported in the researches of Han *et al*. (2005), Lu *et al*. (2009, 2012) and Wang *et al*. (2007).

The concrete constitutive model for reinforcement elements is expressed as follow

$$\sigma = \begin{cases} \sigma_{c0}[\dfrac{s(\varepsilon/\varepsilon_{c0})}{s-1+(\varepsilon/\varepsilon_{c0})^s}] \,, & \varepsilon \le \varepsilon_{c0} \\ \sigma_{c0}\exp[s_1(\varepsilon-\varepsilon_{c0})^{s_2}] \,, & \varepsilon > \varepsilon_{c0} \end{cases} \tag{5}$$

Where σ_c and ε_c are respectively the stress axial strain acting on confined concrete; σ_{c0} and ε_{c0} are respectively the compressive strength in confined concrete and the corresponding axial strain; s is a parameter controlling the slope of the ascending branch and s_1, s_2 are the parameters controlling the stress-strain curve that are expressed as

$$s = \frac{E_c}{E_c - \sigma_{c0} / \varepsilon_{c0}} \tag{6}$$

$$s_1 = \frac{\ln 0.5}{(\varepsilon_{50} - \varepsilon_{c0})^{s_2}} \tag{7}$$

$$s_2 = 1 + 25 I_{e50}^{\,2} \tag{8}$$

Where E_c is the tangent modulus of elasticity of unconfined concrete; ε_{50} is the post-peak strain corresponding to $0.5\sigma_{c0}$; I_{e50} the effective confinement index evaluated at the post-peak strain ε_{50}.

The concrete constitutive model for CFST elements is expressed as follow

$$y = \begin{cases} 2x - x^2 & x \le 1 \\ \dfrac{x}{\beta(x-1)^{\eta} + x} & x > 1 \end{cases} \tag{9}$$

$$x = \frac{\varepsilon_c}{\varepsilon_{c0}} \tag{10}$$

$$y = \frac{\sigma_c}{\sigma_{c0}} \tag{11}$$

$$\beta = \begin{cases} \dfrac{(f_c')^{0.1}}{1.35\sqrt{1+\xi}} & \xi \le 3.0 \\[2mm] \dfrac{(f_c')^{0.1}}{1.35\sqrt{1+\xi(\xi-2)^2}} & \xi > 3.0 \end{cases} \tag{12}$$

$$\eta = 1.6 + 1.5 / x \tag{13}$$

Where $\xi = (A_s / A_c) \cdot (f_y / f_{ck})$ is the confinement factor; f_c' is the cylinder axial compressive strength of concrete; A_s is the sectional area of the steel tube; A_c is the area of the concrete in the tube; f_y is the yield stress of steel; f_{ck} is the prismoidal compressive strength of concrete, $f_{ck} = 0.96 f_c'$; The strain corresponding to the $40\%\sigma_{c0}$ is adopted as the ultimate strain ε_{cu} for the confined concrete in the tube

$$\sigma_{c0} = [1 + (-0.0135\xi^2 + 0.1\xi)(\frac{24}{f_c'})^{0.45}] \cdot f_c' \tag{14}$$

$$\varepsilon_{c0} = (1300 + 12.5 f_c') + [1330 + 760(\frac{f_c'}{24} - 1)] \cdot \xi^{0.2} \quad (\mu\varepsilon) \tag{15}$$

The constitutive model for reinforcement and steel elements is expressed as follow

$$\sigma_s = \begin{cases} E_s \varepsilon_s \ , & \varepsilon_s \leq \varepsilon_y \\ f_y \ , & \varepsilon_y < \varepsilon_s \leq k_1 \varepsilon_y \\ k_4 f_y + \dfrac{E_s(1-k_4)}{\varepsilon_y(k_2-k_1)^2}(\varepsilon_s - k_2 \varepsilon_y)^2 \ , & \varepsilon_s > k_1 \varepsilon_y \end{cases} \tag{16}$$

Where σ_s and ε_s are respectively the stress and corresponding strain; E_s is the elasticity modulus; f_y and $\varepsilon_y = f_y / E_s$ are respectively the yield stress and the yield strain; k_1 is the ratio of the strain corresponding to the starting point of hardening to yield strain; k_2 is the ratio of the strain corresponding to the peak stress to the yield strain; k_3 is the ratio of ultimate strain to the yield strain; k_4 is the ratio of the peak stress to the yield strength. In current research, $k_1 = 4$, $k_2 = 25$, $k_3 = 40$ and $k_4 = 1.2$.
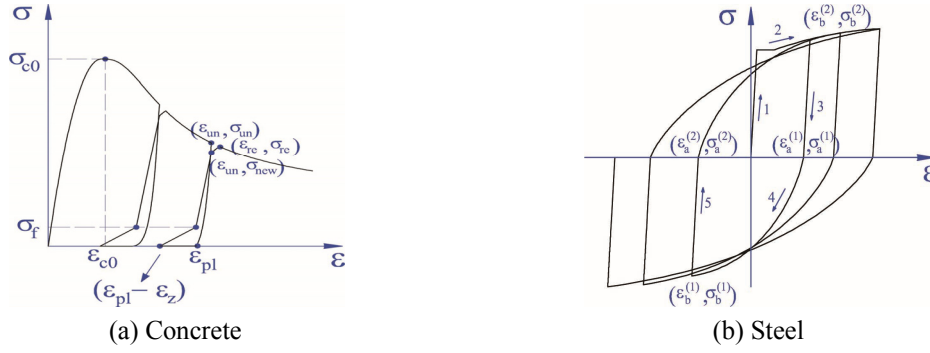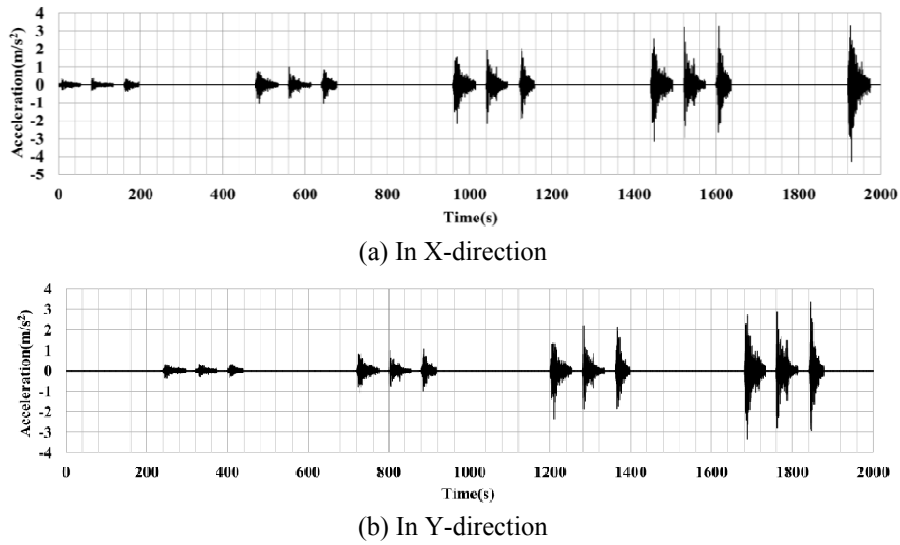

(a) Concrete   (b) Steel

Fig. 18 Constitutive models

(a) In X-direction

(b) In Y-direction

Fig. 19 Earthquake input sequence for numerical simulation

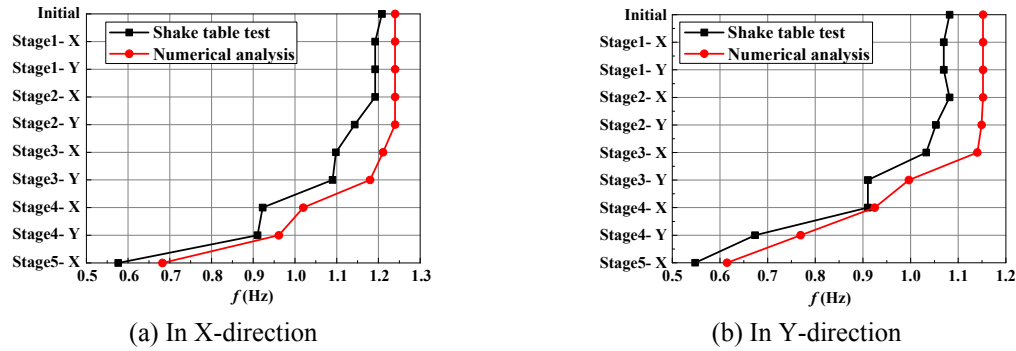(a) In X-direction   (b) In Y-direction

Fig. 20 Comparison of 1st order fundamental frequency change

6.1.3 Earthquake input sequence

Fig. 19 plots the earthquake excitations used in time history analysis of prototype structure that were transformed from the test measurement values obtained from shake table tests base on similitude law.

6.2 Numerical results

Fig. 20 shows the comparison of the 1st order fundamental frequency change between measured values and numerical results. Both of the test and numerical results showed that the fundamental frequencies decreased as the PGA of earthquake excitation increased. The initial measured and calculated 1st order fundamental frequencies were respectively 1.21 Hz and 1.24 Hz in X-direction, and 1.08 Hz and 1.15 Hz in Y-direction. The final measured and calculated 1st order fundamental frequencies were respectively 0.58 Hz and 0.68 Hz in X-direction, and 0.55 Hz and 0.61 Hz in Y-direction.
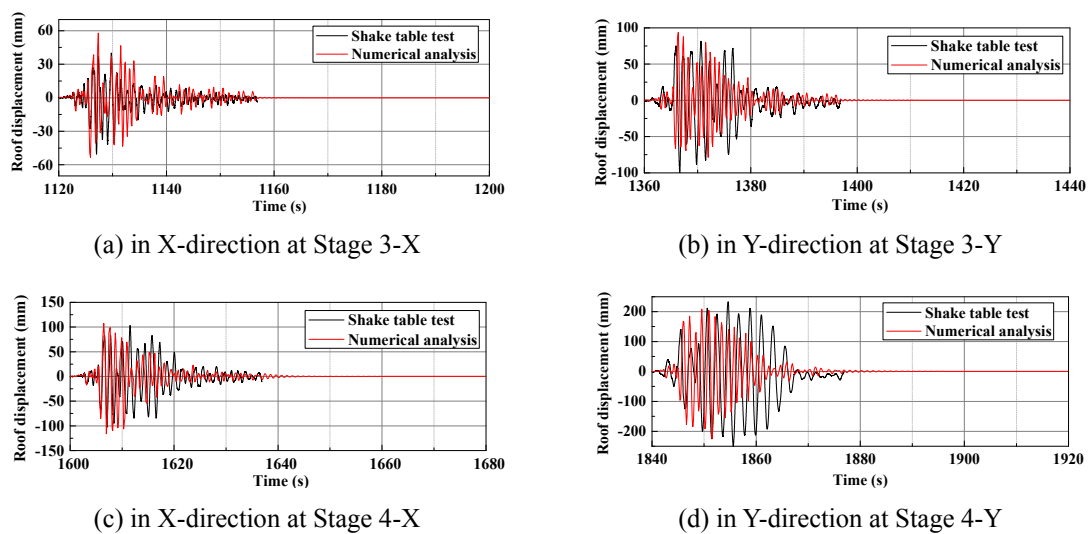

(a) in X-direction at Stage 3-X   (b) in Y-direction at Stage 3-Y

(c) in X-direction at Stage 4-X   (d) in Y-direction at Stage 4-Y

Fig. 21 Comparison of the roof displacements under artificial excitation

(a) base to 1st floor.
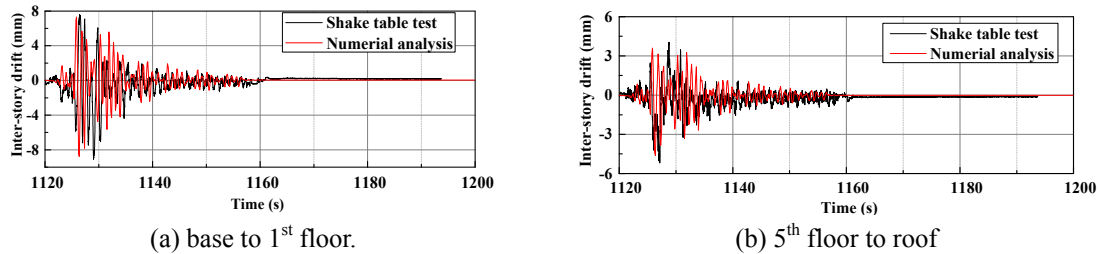

(b) 5th floor to roof

Fig. 22 Comparison of the inter-story drift under artificial excitation in X-direction at Stage 3-X
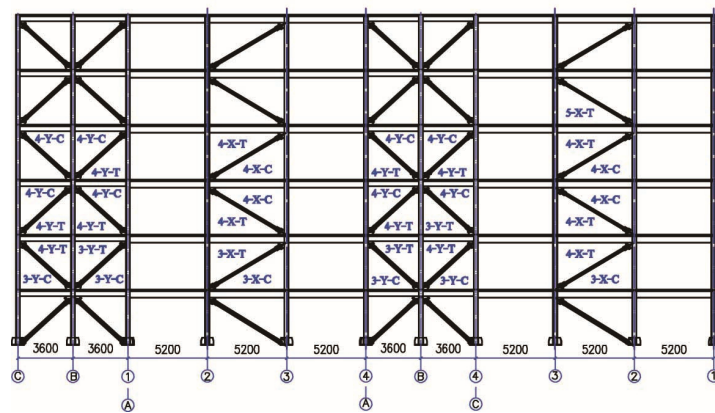

Fig. 23 Comparison of progressive failure of the brace system between experimental and numerical study
* Mark represents "stage-direction-method". For example, "4-Y-C" represents that this brace fails at Stage 4-Y during calculation, "3-X-T" represents that this brace fails at Stage 3-X during test

Figs. 21-22 plot some typical calculated displacement responses compared with test measurement values. Since Stage 5, the calculated displacement response attenuated faster than the measured displacement value after the displacement reaches to the maximum value. But the numerical method can properly simulate the vibration characteristics of prototype, the calculated maximum displacements, and inter-story drifts.

Fig. 23 illustrates the progressive failure sequence of the CFST brace system during shake table tests and numerical analysis. In the first place, CFST braces began to fail in 2nd floor at Stage 3 in X-direction, then the damage extended to upper floors as the PGA of the seismic excitation increased. The calculated and observed failure sequence of the braces and the stages where they failed were basically the same.

There were some discrepancies between the measured and calculated results, which should be caused due to the following factors: (1) fabrication errors of test model; (2) discrepancy of material property; (3) measurement noise; (4) finite stiffness of the shake table; and (5) simplifications of the boundary conditions and material constitutive relations for numerical model, for example, the column to beam, plate to beam, column base connections were taken to be ideally fixed. However, the overall comparisons indicate that the discrepancies are acceptable, the numerical model can properly simulate the dynamic property and responses of the precast CFSTC-RCB braced frame that are highly concerned in engineering practice.

7. Conclusions

To investigate the global seismic performance of the proposed new precast CFSTC-RCB braced frame, a series of shake table tests and numerical time history analysis were conducted. According to the measured and calculated results, the main conclusions are summarized as follows:

- After a CFST brace failing, plastic hinges subsequently appeared on some of the composite beams that were adjacent to this brace, while the CFST column sustained excellent performance in the overall process of earthquake excitation. Therefore, the "strong CFST column-weak RC beam" anti-seismic design principle can be easily achieved.
- Plastic hinges on composite beams appeared at interfaces between the RC beam segment and SC beam segment, which had a considerable distance to the core region of column to beam connection, thus achieving the expected goal to maintain the integrity of the column to beam connection. No damage were found at the column to beam connection region even after the composite beams and CFST braces were severely damaged, the "strong connection-weak member" anti-seismic design principle can be easily achieved.
- Under the frequent, occasional and rare earthquake excitations, the maximum deflections of precast CFSTC-RCB braced frame satisfied the deflection limitations in national code. Under the extremely rare earthquake excitations that are not required by national code, a few local maximum inter-story drifts surpassed the deflection limitations, but the CFST columns and connections still worked well and no sign of global collapse was observed.
- During earthquake excitations, the loss of CFST braces can result in considerable stiffness degradation in the floors where braces failed, the inter-story drifts in these floors were greater than the inter-story drifts in other floors, which should be carefully considered in structural design.
- It has been shown that the failure of the CFST braces were generally due to the deformation of end plates and the cutting off of the high-strength bolts. Therefore, the connection strength between the CFST braces and column to beam connections should be further improved so that the failure location in the CFST brace system can transfers to the main body of the CFST braces, which can further optimize the seismic performance of the new precast CFSTC-RCB braced frame and avoid excessive material and repair cost.
- The comparison between the calculated and measured values have shown that the numerical model can properly simulate the dynamic properties and responses of the precast CFSTC-RCB braced frame that are highly concerned in engineering practice.

Acknowledgments

References

Bai, Y., Nie, J.G. and Cai, C.S. (2008), "New connection system for confined concrete columns and beams.II:Theoretical modeling", *J. Struct. Eng.*, **134**(12), 1800-1809.
GB 50010-2010 (2010), Code for design of concrete structures, Ministry of Housing and Urban-Rural

Development of the People's Republic of China, Beijing, China.

GB 50011-2010 (2010), Code for seismic design of buildings, Ministry of Housing and Urban-Rural Development of the People's Republic of China, Beijing, China.

GB 50017-2003 (2003), Code for design of steel structures, Ministry of Housing and Urban-Rural development of the People's Republic of China, Beijing, China.

Han, L.H., Zhao, X.L. and Tao, Z. (2001), "Tests and mechanics model of concrete-filled SHS stub columns, columns and beam-columns", *Steel Compos. Struct.*, *Int. J.*, **1**(1), 51-74.

Han, L.H., Yao, G.H. and Zhao, X.L. (2005), "Tests and calculations for hollow structural steel (HSS) stub columns filled with self-consolidating concrete (SCC)", *J. Construct. Steel Res.*, **61**(9), 1241-1269.

Han, L.H., Wang, W.H. and Yu, H.X. (2010), "Experimental behavior of reinforced concrete(RC) beam to concrete-filled steel tubular(CFST) column frames subjected to ISO-834 standard fire", *Eng. Struct.*, **32**(10), 3130-3144.

Légeron, F. and Paultre, P. (2003), "Uniaxial confinement model for normal and high-strength concrete columns", *J. Struct. Eng.*, **129**(2), 241-252.

Li, S. (2013), "Studies on method for modal parameter identification and damage identification of engineering structure", Ph.D. Dissertation; Chongqing University, Chongqing, China.

Li, G.C., Fang, C., An, Y.W. and Zhao, X. (2015), "Seismic behavior of rebar-penetrated joint between GCFST column and RGC beam", *Steel Compos. Struct.*, *Int. J.*, **19**(3), 547-567.

Liao, F.Y., Han, L.H. and Tao, Z. (2014), "Behaviour of composite joints with concrete encased CFST columns under cyclic loading: Experiments", *Eng. Struct.*, **59**, 745-764.

Lu, X.Z., Lin, X.C., Ma, Y.H., Li, Y. and Ye, L.P. (2008), "Numerical simulation for the progressive collapse of concrete building due to earthquake", *Proceedings of the 14th World Conference on Earthquake Engineering*, Beijing, China, October.

Lu, X.Z., Ye, L.P. and Liao, Z.W. (2009), *Elasto-plastic Analysis of Buildings Against Earthquake-theory*, *Model and Implementation on ABAQUS, MSC.MARC and SAP2000*, China Architecture and Building Press, Beijing, BJ, China.

Lu, X.Z., Lu, X., Guan, H., Zhang, W.K. and Ye, L.P. (2012), "Earthquake-induced collapse simulation of a super-tall mega-braced frame-core tube building", *J. Construct. Steel Res.*, **82**, 59-71.

MSC.Marc (2010a), *MSC.Marc Volume B: Element Library*, MSC.Software Corp., Santa Ana, CA, USA.

MSC.Marc (2010b), *MSC.Marc Volume D: User Subroutines and Special Routines*, MSC.Software Corp., Santa Ana, CA, USA.

Nie, J.G., Bai, Y. and Cai, C.S. (2008), "New connection system for confined concrete columns and beams. I: Experimental study", *J. Struct. Eng.*, **134**(12), 1787-1799.

Qu, H. (2012), "Mechanical analysis of reinforced beam - CFST column joint under seismic loading", *Eng. Mech.*, **29**(7), 235-243.

Ren, P.Q., Li, Y., Guan, H. and Lu, X.Z. (2015), "Progressive collapse resistance of two typical high-rise RC frame shear wall structures", *J. Perform. Construct. Facil.*, **29**(3), 04014087.

Sun, X.L. (2009), "Experimental research on seismic behavior of single span concrete-filled steel tubular frame with reinforced concrete beams", *J. Build. Struct.*, **30**(1), 142-146+156.

Tan, Q.H., Han, L.H. and Yu, H.X. (2012), "Fire performance of concrete filled steel tubular (CFST) column to RC beam joints", *Fire Safe. J.*, **51**, 68-84.

Wang, X.L., Lu, X.Z. and Ye, L.P. (2007), "Numerical simulation for the hysteresis behavior of RC columns under cyclic loads", *Eng. Mech.*, **24**(12), 76-81.

Zhang, Y.F., Zhao, J.H. and Cai, C.S. (2012), "Seismic behavior of ring beam joints between concrete-filled twin steel tubes columns and reinforced concrete beam", *Eng. Struct.*, **39**, 1-10.

BU